Flow Enhancement and Reduction in Pulsatile Flow of Discotic Nematic Liquid Crystals

Luiz R.P. de Andrade Lima; Alejandro D. Rey
Department of Chemical Engineering, McGill University
3610 University Street, Montreal, Quebec, Canada H3A 2B2
e-mail: ldeand@po-box.mcgill.ca; alejandro.rey@mcgill.ca

Abstract

An important feature of nematic liquid crystals is the coupling between the orientation and velocity fields that results in flow-induced orientation and re-orientation induced flow. Due to the viscoelastic nature of the material this coupling can have an effect on the effective flow rate of pulsatile flow. In the present study, the pulsating flow of uniaxial, isothermal, incompressible discotic nematic liquid crystals in a capillary is analyzed using the Leslie-Ericksen equations. The computations were done by using the Galerkin finite element methods for space discretizations and 4^{th} order Runge-Kutta method for time integration. The results indicate that flow-rate-enhancement or flow-rate reduction are possible, according to the magnitude of the average pressure drop. The fundamental mechanisms that lead to flow-rate enhancement and reduction are established using liquid crystal physics. The role of pressure drop amplitude and oscillation frequency on flow-rate is characterized and explained using principles of nematodynamics. The role of shear thinning and shear thickening behavior on flow-rate enhancement and reduction is established.

Introduction

Pulsatile flows of non-Newtonian fluids have attracted wide interest due to potential uses as a characterization tool, optimization of pressure-driven processing flows, and applications in biofluid mechanics [1,2,3]. A widely studied oscillatory flow is pressure-driven pulsatile capillary Poiseuille flow, were the pressure-drop undergoes temporal harmonic oscillations, and relative flow-enhancement over the steady values is characterized as a function of pressure-drop amplitude, frequency, and base value. Shear-dependent viscosities and internal relaxation times are examples of properties accessible through pulsatile flow. If power input increases at a lower rate than flow-enhancement does, then this transient flow provides energy savings with respect to steady flows.

The pulsatile flow of viscoelastic liquids and viscoplastic suspensions have been widely analyzed theoretically and experimentally and the mean flow rate enhancement has been characterized [1,4,5,6]. Theoretical predictions of mean flow rate enhancement as a function of frequency and amplitude of pressure-drop oscillation has been evaluated for many constitutive equations. These pulsatile flow studies found that shear-thinning causes flow-enhancement, and that the flow enhancement is proportional to the square of the relative amplitude of the oscillating pressure gradient. For viscoplastic materials, it was found that the flow rate enhancement is independent of the frequency but proportional to the square of the amplitude the oscillating pressure gradient. Based on previous work, it can be concluded that flow-enhancement may be driven by: inertia, and shear thinning. On the other hand the frequency dependence of flow-enhancement is due to viscoelasticity. This paper presents a computational study of a model liquid crystalline viscoelastic material, that exhibits both shear-thinning and shear-thickening, and hence flow-reduction and flow-enhancement are predicted.

In addition the presence of a single relaxation time results in resonance when the externally applied frequency is close to orientation time scale.

Uniaxial discotic nematic liquid crystals (DNLCs), here denoted as discotic mesophases (DMs) are characterized by an average molecular orientation represented by the director vector **n**. In this phase the unit normals to the disk-like molecules orient close to the director **n** [7]. Simulations and experiments indicates that the apparent viscosity in steady Poiseuille flow can be of the shear thinning type or non-monotonic, depending on the adopted orientation [8]. Natural and synthetic mesophase pitches, which are precursor used in the manufacturing of high performance carbon fiber by the melt spinning process, are examples of discotic nematic liquid crystals; also highly filled clay-based polymer nano-composites are expected to display nematic ordering.

Transient nematic flows are characterized by the presence of three important viscoelastic phenomena [9]: backflows, viscosity reduction mechanisms, and transient re-orientation effects on velocity. Backflow is the inverse of flow-induced orientation, and is most dramatic in cessation of flow, where the stored elastic energy is dissipated by viscous flow. Viscosity reduction occurs when the director rotates in an otherwise steady flow, and is another manifestation of orientation-induced flow. When the amplitude of the re-orientation is small the viscosity reduction is given by a simple combination of material properties, but when the amplitude is large the reduction is a non-linear function of the director field. Transient director re-orientation will affect the velocity since the viscosity is orientation dependent. In simple shear flows this effect is quantified by the stress overshoot measurements, while in transient Poiseuille flows it will be quantified by the flow rate [8,10].

This paper characterizes flow-enhancement in capillary pulsatile Poseuille flow of a model discotic nematic liquid crystal, identify flow-enhancement and flow-reduction mechanisms driven by liquid crystalline order, and anisotropic viscoelasticity, and identifies specific viscoelastic material properties that have the largest impact on flow-enhancement.

Governing Equations

In flowing liquid crystal systems, elastic and viscous stresses are usually both important. The continuum theory of elasticity of liquid crystals takes into account external forces that distort the spatially uniform equilibrium configurations of liquid crystals. For Poiseuille capillary flow, using cylindrical coordinate system, Fig.1, axisymmetric planar director field ($\mathbf{n}(r,t)=(\sin\theta(r,t),0,\cos\theta(r,t))$) and purely axial velocity field ($\mathbf{v}(r,t)=(0,0,v(r,t))$) the dimensionless governing equations for the director tilt angle $\theta(\tilde{r},\tilde{t})$ and the axial velocity $\tilde{v}(\tilde{r},\tilde{t})$ are [8,10]:

$$\frac{\partial\theta}{\partial\tilde{t}}=\frac{\left(\cos^2\theta+\varepsilon\sin^2\theta\right)}{\tilde{\Upsilon}(\theta)}\left[\frac{\partial^2\theta}{\partial\tilde{r}^2}+\frac{1}{\tilde{r}}\frac{\partial\theta}{\partial\tilde{r}}\right]+\frac{\sin2\theta}{2\tilde{\Upsilon}(\theta)}\left[(\varepsilon-1)\left(\frac{\partial\theta}{\partial\tilde{r}}\right)^2-\frac{1}{\tilde{r}^2}\right]-\left[\frac{\tilde{U}(\theta)E}{2\ \tilde{G}(\theta)\tilde{\Upsilon}(\theta)}\right]\tilde{r} \qquad (1)$$

$$\frac{\partial\tilde{v}}{\partial\tilde{r}}=-\left(\frac{\tilde{r}}{2\tilde{G}(\theta)}\right)E+\ \tilde{B}\left(\theta,\frac{\partial\theta}{\partial\tilde{t}}\right) \qquad (2)$$

$$\tilde{\Upsilon}(\theta) = \tilde{\gamma}_1 - \frac{\tilde{U}^2(\theta)}{\tilde{G}(\theta)} \tag{3}$$

$$\tilde{G}(\theta) = \tilde{\alpha}_1 \sin^2\theta\cos^2\theta + \tilde{\eta}_1\cos^2\theta + \tilde{\eta}_2\sin^2\theta \tag{4}$$

$$\tilde{U}(\theta) = \tilde{\alpha}_2\sin^2\theta - \tilde{\alpha}_3\cos^2\theta \tag{5}$$

$$\tilde{B}\left(\theta, \frac{\partial\theta}{\partial\tilde{t}}\right) = \left(\frac{\tilde{U}(\theta)}{\tilde{G}(\theta)}\right)\frac{\partial\theta}{\partial\tilde{t}} \tag{6}$$

$$\tilde{\eta}_1 = \eta_1 / \langle\eta\rangle, \qquad \tilde{\eta}_2 = \eta_2 / \langle\eta\rangle, \qquad \tilde{\eta}_3 = \eta_3 / \langle\eta\rangle \tag{7}$$

$$\langle\eta\rangle = \frac{\eta_1+\eta_2+\eta_3}{3} \tag{8}$$

$$\eta_1 = (\alpha_3 + \alpha_4 + \alpha_6)/2\ , \qquad \eta_2 = (-\alpha_2 + \alpha_4 + \alpha_5)/2\ , \qquad \eta_3 = \alpha_4/2 \tag{9}$$

where $\tilde{\alpha}_i$ are the dimensionless Leslie viscosities ($\tilde{\alpha}_i = \alpha_i/\langle\eta\rangle$), $\langle\eta\rangle$ is the average Miesowicz viscosity, $\varepsilon = K_{33}/K_{11}$ is the ratio of the bend and the splay Frank elastic constants, $E = R^3(-dp/dz)/K_{11}$ is the ratio of viscous flow effects to long-range elasticity effects known as the Ericksen number, $\tilde{r} = r/R$ is the dimensionless radius, R is the capillary radius, $\tilde{t} = K_{11}t/(R^2\langle\eta\rangle)$ is the dimensionless time, $\tilde{v} = \langle\eta\rangle R\, v/K_{11}$ is the scaled axial velocity, $-dp/dz$ is the given pressure drop in the capillary per unit length, $\tilde{B}$ is the dimensionless backflow, $\tilde{G}(\theta)$ is the dimensionless local viscosity function, $\tilde{\Upsilon}(\theta)$ is the dimensionless re-orientation viscosity and $\tilde{U}(\theta)/\tilde{G}(\theta)$ is the backflow dimensionless viscosity function.

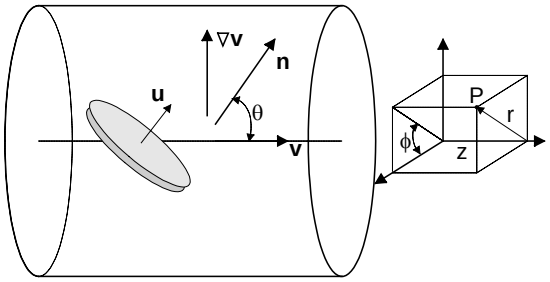

Figure 1. Schematic representations of the flow in a capillary showing an uniaxial disc-like molecules with unit normal vector (**u**), director vector (**n**), velocity vector (**v**), velocity gradient (∇**v**), alignment angle (θ) and the cylindrical (r,ϕ,z) coordinate system used to describe a generic point P.

Under oscillatory pulsatile flow, the pressure drop (–dp/dz) oscillates with amplitude A, frequency ω, around a mean $\langle -dp/dz\rangle$:

$$-\frac{dp}{dz}(A,\omega,t) = \left\langle -\frac{dp}{dz}\right\rangle(1 + A\sin\omega t) \tag{10}$$

and the dimensionless solution vector to Eq.(1) and (2) is given by:

$$\tilde{v} = \tilde{v}\left(\tilde{r}, \tilde{t}, E\left(A, \tilde{\omega}, \tilde{t}\right)\right),\ \theta = \theta\left(\tilde{r}, \tilde{t}, E\left(A, \tilde{\omega}, \tilde{t}\right)\right),\ E\left(A, \tilde{\omega}, \tilde{t}\right) = E_o\left(1 + A\sin\tilde{\omega}\tilde{t}\right),\ E_o = \frac{R^3}{K_{11}}\left\langle -dp/dz\right\rangle \qquad (11)$$

where $E\left(A, \tilde{\omega}, \tilde{t}\right)$ is now the transient Ericksen number, E_o is the average Ericksen number, $\left\langle -dp/dz\right\rangle$ is the average pressure-drop, $\tilde{\omega} = \omega\left(R^2\left\langle\eta\right\rangle\right)/K_{11}$ is the dimensionless frequency. Note that the frequency ω is scaled with the orientation time scale τ_o:

$$\tau_o = \left(R^2\left\langle\eta\right\rangle\right)/K_{11} \qquad (12)$$

Under steady capillary Poiseuille flow, $E=E_o$, $A=0$ and the solution vector is given by:

$$\tilde{v}_s = \tilde{v}_s\left(\tilde{r}, E_o\right),\quad \theta_s = \theta_s\left(\tilde{r}, E_o\right),\ E_o = \frac{R^3}{K_{11}}\left(-dp/dz\right)_s \qquad (13)$$

Equation (1) is a parabolic partial differential equation, whereas the Eq (2) is a first order space dependent ordinary differential equation (ODE). The Eq. (1) is independent of Eq.(2) and hence the governing equations are semi-coupled. Since inertia is neglected in the linear momentum balance, no initial condition on the velocity can be imposed since it is an ODE. The boundary conditions for Eq.(1) are: ($\theta(0,\tilde{t}) = \theta(1,\tilde{t}) = 0$), and represent strong planar anchoring. For the Eq.(2) the no slip condition at the bounding surface is used: $\tilde{v}(1,\tilde{t}) = 0$.

The calculations presented here are performed using a set of characteristic DMs viscoelastic material parameters listed in Table 1, which correspond to the six scaled Leslie coefficients calculated to carbonaceous mesophase [12]. The essential features of the solutions and the main conclusions of this paper will remain unaffected if the reactive parameter ($\lambda = -\left(\alpha_3 + \alpha_2\right)/\left(\alpha_3 - \alpha_2\right)$) is less than minus one and if the Miesowicz inequalities ($\eta_1 > \eta_3 > \eta_2$) hold.

Table 1: Viscoelastic Parametric Values

Dimensionless Leslie viscosities coefficients ($\tilde{\alpha}_i = \alpha_i/\left\langle\eta\right\rangle$)	
$\tilde{\alpha}_1$	3.6289
$\tilde{\alpha}_2$	0.046800
$\tilde{\alpha}_3$	0.66500
$\tilde{\alpha}_4$	2.0270
$\tilde{\alpha}_5$	-0.54000
$\tilde{\alpha}_6$	0.17200
Elastic ratio	
ε	0.66667

Equation (1) is solved numerically using the Galerkin Finite Element method for spatial discretization and finite differences for temporal discretization [13]. The spatial discretization uses 200 to 250 linear elements and a non-uniform mesh, with a larger node density in the center and at the capillary walls. For time integration we used the 4th order explicit Runge-Kutta method with a fixed time step of $1.5\text{x}10^{-7}$ to $2.8\ \text{x}10^{-7}$; the integrals were computed using

three points Gaussian quadrature and the resulting set of non-linear equations are solved using the Newton-Raphson iteration scheme. The numerical convergence is assumed to occur when the length of the difference between two successive solutions vectors is less than 10^{-10}, and the mesh independence was established using standard mesh refinement criteria. Equation (2) and the flow-rate in the capillary are calculated using three points Gaussian quadrature. A typical calculation proceeds as follows. Initially, the Ericksen number is set equal to the average value E_o, to assure that the pulsatile flow will arise only after the orientation is at the steady state, which is reached when the difference between two successive solution vectors is less than 10^{-8}. Next, the moving average flow-rate for an oscillation cycle is calculated using three points Gaussian quadrature. We assume that convergence is achieved when the difference between the larger and the lower values of the flow rate in the cycle is less than 0.01, and the final value of the flow rate is taken to be the average between these two nearly identical values.

Flow-Enhancement

Flow-enhancement is defined as the relative flow rate change with respect to the steady state flow rate, for a given average pressure drop, amplitude A, and frequency ω. In dimensionless form the flow-enhancement is given by:

$$I\left(A, \tilde{\omega}, E_o\right) = \frac{\left\langle \tilde{Q} \right\rangle - \tilde{Q}_s\left(E_o\right)}{\tilde{Q}_s\left(E_o\right)} \quad , \quad \left\langle \tilde{Q} \right\rangle = f\left(A, \tilde{\omega}, E_o\right) \tag{14}$$

where the dimensionless steady state flow rate $\tilde{Q}_s\left(E_o\right)$ is given by:

$$\tilde{Q}_s\left(E_o\right) = 2\pi \int_0^1 \tilde{v}_s\left(\tilde{r}, E_o\right) \tilde{r} d\tilde{r} \tag{15}$$

and the dimensionless average flow-rate $\left\langle \tilde{Q} \right\rangle$ is:

$$\left\langle \tilde{Q} \right\rangle = \frac{2\pi}{\tilde{\tau}} \int_0^{\tilde{\tau}} \left(\int_0^1 \tilde{v}\ \left(\tilde{r}, u, A, \tilde{\omega}, E_o\right) \tilde{r} d\tilde{r} \right) du = f\left(A, \tilde{\omega}, E_o\right), \quad \tilde{\tau} = \frac{2\pi}{\tilde{\omega}} \tag{16}$$

and $\tilde{\tau}$ is the cycle period.

To characterize the mechanism responsible for flow-enhancement we must use the dimensionless apparent steady viscosity:

$$\tilde{\eta}_{app,s}\left(E_o\right) = \frac{\pi\ E_o}{8\ \tilde{Q}_s\left(E_o\right)} \tag{17}$$

and the following viscoelastic properties: Miesowicz viscosities, reactive parameter, and the re-orientation viscosities [8,10].

Numerical results and discussion

Figure 2 shows the steady director angle θ as a function of dimensionless distance $\tilde{r}$, for E_o= 1, 10, 10^2, 10^3 and 10^4, and A=0. The figure shows that large orientation profiles distortions occur for $10<E_o<10^4$. For $E_o>10^4$, the system is flow-aligned, while for $E_o<10$, there

is little distortion. Figure 2 also shows the corresponding steady dimensionless velocity $\tilde{v}_s(\tilde{r})$ as a function of a function of dimensionless distance $\tilde{r}$. For $E_o>10^4$, and $E_o<10$ the velocity profile is parabolic (Newtonian). Note that the viscoelasticty is significant within the interval $10<E_o<10^4$.

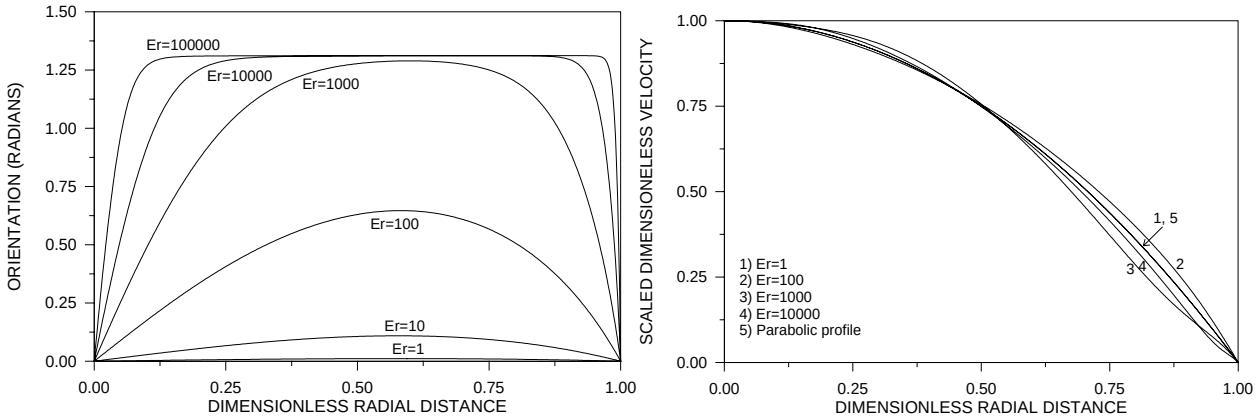

Figure 2. Steady director angle θ as a function of dimensionless distance $\tilde{r}$, for E_o= 1, 10, 10^2, 10^3 and 10^4, and A=0.

Figure 3 shows the steady dimensionless apparent viscosity $\tilde{\eta}_{app,s}$ and the flow rate enhancement I as a function of the average Ericksen number E_o in pulsating flow, for A=0.5, 1, and $\tilde{\omega}$=50. The viscosity is shear-thickening and thinning [8]. The interval of viscosity changes is $10<E_o<10^4$. The figure shows that flow-enhancement in DNLCs is negative in the shear-thickening region, and positive in the shear-thinning region. The Newtonian cross-over (I=0) is close to the viscosity maximum: $d\eta_{app,s}/dE_o = 0$, and nearly to amplitude-independent. Note that increasing amplitude increases the magnitude of I. Increasing frequency decreases the magnitude of I. The cross-over ($I(E_o=E_N)=0$) is nearly independent of amplitude and frequency.

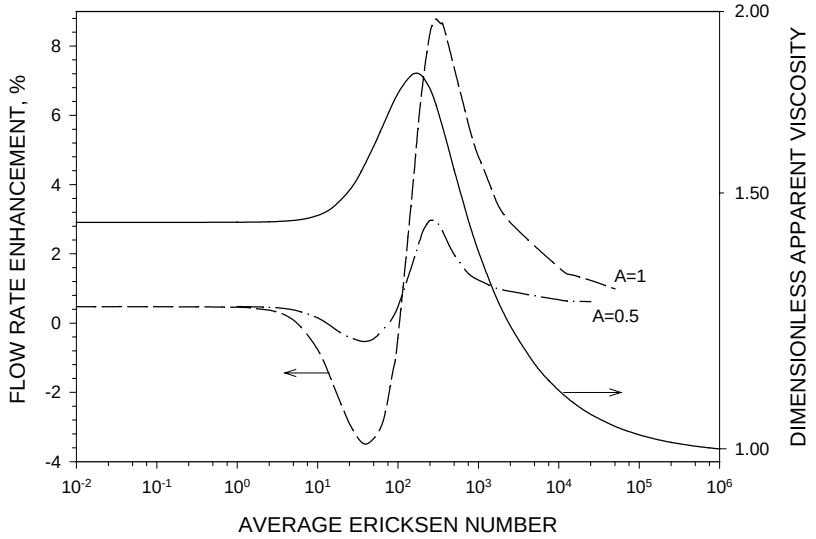

Figure 3. Steady dimensionless apparent viscosity $\tilde{\eta}_{app,s}$ and the flow rate enhancement I as a function of the average Ericksen number E_o in pulsating flow, for A=0.5, 1, and $\tilde{\omega}$=50.

The figures show the following response:

- Asymptotic Newtonian regime, $E_0 \to 0 : I \to 0$
- Flow-reduction regime, $0 < E_0 < E_N = 100 : I < 0$
- Newtonian cross-over, $E_0 = E_N = 100 : I = 0$
- Flow-enhancement regime, $E_0 > E_N = 100 : I > 0$
- Asymptotic Newtonian regime, $E_0 \to \infty : I \to 0$

For very high or very small E_o, the behavior is Newtonian and I=0.

To explain the underlying mechanism that drives flow-enhancement and flow-reduction one focus on the oscillating director and velocity profiles, across one cycle. Figure 4a shows the local dimensionless viscosity function $\tilde{G}\left(\theta\left(\tilde{r},\tilde{t}\right)\right)$ for one oscillation cycle, corresponding to the flow-reduction regime (E_o=50<E_N), for A=1, and $\tilde{\omega}$=100. The profiles cycle between two cubic with a local maxima in the interval $0.6 < \tilde{r} < 0.7$. At $\tilde{r} = 0,1$, the director is fixed along the flow-direction and the viscosity is: $\tilde{G}\left(\theta\left(0,\tilde{t}\right)\right) = \tilde{G}\left(\theta\left(1,\tilde{t}\right)\right) = \tilde{\eta}_l = 1.43$. In this regime the viscosity function profile oscillates as follows:

$$E_o < E_N, \qquad \tilde{\eta}_l < \tilde{G}(\theta) < \tilde{G}_{max}(\theta_{max}) \tag{18}$$

At these pressure-drops there is no flow-alignment and the local viscosity is high. Figure 4a shows the local dimensionless viscosity function $\tilde{G}\left(\theta\left(\tilde{r},\tilde{t}\right)\right)$ for one oscillation cycle, corresponding to the flow-reduction regime close to the Newtonian cross-over (E_o=E_N) at which flow-enhancement vanishes, for A=1, and $\tilde{\omega}$=100. Note that these profiles cycle between a cubic and a curve with two local maxima and a local minimum. At $\tilde{r} = 0,1$, the director is fixed along the flow-direction, the viscosity is: $\tilde{G}\left(\theta\left(0,\tilde{t}\right)\right) = \tilde{G}\left(\theta\left(1,\tilde{t}\right)\right) = \tilde{\eta}_l$. In this cross-over the viscosity function profile oscillates as follows:

$$E_o \approx E_N, \qquad \tilde{\eta}_l < \tilde{G}(\theta) = \tilde{G}_{max}(\theta_{max}) \tag{19}$$

The viscosity now samples its maximum value, but in the interval $\tilde{r} \approx 0.3 - 0.9$, a viscosity reduction sets since the director attains angles closer to θ_{al}=1.31, which are associated with lower viscosity. Hence the underlying mechanism operating at the Newtonian cross-over is the orientation-dependent local viscosity. As the pressure drop increases across the transition value, an annular region arises periodically, where director oscillates increasingly closer to the flow-alignment. Figure 4c shows the local dimensionless viscosity function $\tilde{G}\left(\theta\left(\tilde{r},\tilde{t}\right)\right)$ for one oscillation cycle, close (E_o=500>E_N) at which flow-enhancement is positive, for A=1, and $\tilde{\omega}$=100. The profiles cycle between two curves with two maxima and a local minimum, corresponding to a three regions: core region, intermediate annular region, and wall region. In the annular region the viscosity cycles between $\tilde{G}_{max}(\theta_{max})$ and $\tilde{G}_{al}(\theta_{al})$. The decrease in viscosity in the annular region drives the flow-enhancement process. Figure 4d shows the scaled Ericksen number $\left(\left(E\left(\tilde{\omega}\tilde{t}\right)/E_o - 1\right)/A\right)$ as a function of $\tilde{\omega}\tilde{t}$, across one cycle. These figures also show the geometrical features and amplitude changes that lead to flow-

enhancement. In the flow-reduction regime, the annular region corresponds to high viscosity and its area is nearly constant, while the inner core is low viscosity. In the Newtonian cross-over the geometry and intensity change, such that the variable width annular region pulsates between higher and lower viscosities. In the flow-enhancement region, the variable width annular region annular region corresponds to low viscosity.

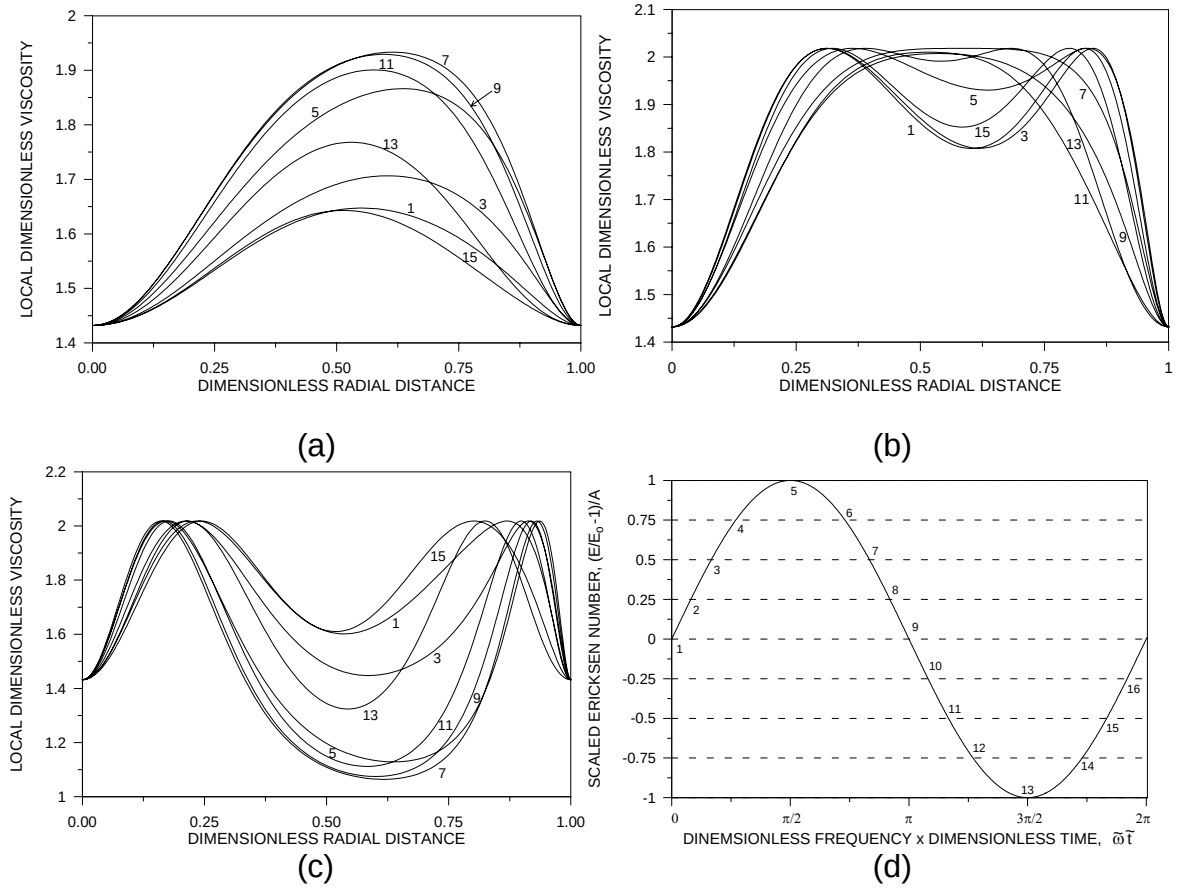

Figure 4. Local dimensionless viscosity function $\tilde{G}\left(\theta\left(\tilde{r},\tilde{t}\right)\right)$ for one oscillation cycle for A=1, and $\tilde{\omega}$=100: (a) (E_o=50<E_N), (b) (E_o=E_N), (c) (E_o=500>E_N). (d) Scaled Ericksen number $\left(\left(E\left(\tilde{\omega}\tilde{t}\right)/E_o\text{-}1\right)/A\right)$ as a function of $\tilde{\omega}\tilde{t}$, across one cycle.

Conclusions

Discotic nematic liquid crystals and anisotropic viscoelastic materials, and the orientation-dependent shear viscosity is a physical property that can result in Non-Newtonian responses. In pressure-driven capillary Poiseuille flow, the apparent viscosity is non-monotonic, and exhibits shear thickening followed shear-thinning behavior. This unusual behavior is a direct result of orientation-dependent viscosity. Under pulsatile flow, this mechanism gives rise to flow-reduction followed by flow-enhancement. The mechanism responsible for shear thickening in steady flow, is responsible to flow-reduction in pulsatile flow. The mechanism responsible for shear thinning in steady capillary Poiseuille flow, is responsible to flow-enhancement in pulsatile flow.

Acknowledgments

This research was supported by a grant from Engineering Research Center program of National Science Foundation under award number EEC 9731680. One of us (LRPdAL) also gratefully acknowledges the support of Natural Sciences and Engineering Research Council of Canada, and the Eugenie Ulmer Lamothe Scholarship Fund (Department of Chemical Engineering, McGill University).

References

[1] R.B. Bird, R.C. Armstrong, and O. Hassager, *Dynamics of Polymeric Liquids*, (John Wiley & Sons: New York, 1987).

[2] J.K-J Li, *Dynamics of the Vascular System*, (World Scientific: Singapore, 2004).

[3] M. Zamir, *The Physics of Pulsatile Flow*, (Springer-Verlag: New York, 2000).

[4] H.A.M. Barnes, P. Townsend, and K. Walters, "On pulsatile flow of non-Newtonian liquids", *Rheological Acta*, **10**, 517 (1971).

[5] M.F. Edwards, D.A. Nellist and W.L. Wilkinson, "Unsteady, laminar flows of non-Newtonian fluids in pipes", *Chemical Engineering Science*, **27**, 295 (1972a).

[6] N. Phan-Thien, and J. Dudek, "Pulsating flow revisited", *Journal of Non-Newtonian Fluid Mechanics*, **11**, 147 (1982).

[7] F. R. S. Chandrasekhar, *Liquid Crystals*, (2nd edn., Cambridge University Press, 1992).

[8] L.R.P. de Andrade Lima and A.D. Rey, "Poiseuille flow of Leslie-Ericksen discotic liquid crystals: solution mutliplicity, multistability, and non-newtonian rheology", *Journal of Non-Newtonian Fluid Mechanics*, **110**(2-3), 103 (2003a).

[9] A.D. Rey and M.M. Denn, "Dynamical phenomena in liquid-crystalline materials", Annual Reviews in Fluid Mechanics, **34**, 233 (2002).

[10] L.R.P. de Andrade Lima and A.D. Rey, "Linear and nonlinear viscoelasticity of discotic nematics under transient Poiseuille flows", *Journal of Rhelogy*, **47**(5), 1261 (2003b).

[11] P.G. de Gennes and J. Prost, *The Physics of Liquid Crystals*, (2nd edn., Oxford University Press, London, 1993).

[12] D. Grecov and A.D. Rey, "Computational rheology for discotic nematic liquid crystals", *Molecular Crystals Liquid Crystals*, **391**, 57 (2003).

[13] C.A.J. Fletcher *Computational Techniques for Fluid Dynamics 1: Fundamental and General Techniques,* (Springer-Verlag: New York, 1996).